Open Access

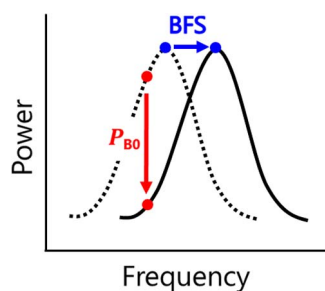# Slope-Assisted Brillouin Optical Correlation-Domain Reflectometry: Proof of Concept

Heeyoung Lee
Neisei Hayashi
Yosuke Mizuno, Member, IEEE
Kentaro Nakamura, Member, IEEE

Slope-Assisted Brillouin Optical Correlation-Domain Reflectometry: Proof of Concept

Heeyoung Lee,[1] **Neisei Hayashi,**[2] **Yosuke Mizuno,**[1] *Member, IEEE*, **and Kentaro Nakamura,**[1] *Member, IEEE*

[1]Laboratory for Future Interdisciplinary Research of Science and Technology, Tokyo Institute of Technology, Yokohama 226-8503, Japan
[2]Research Center for Advanced Science and Technology, University of Tokyo, Tokyo 153-8904, Japan

Abstract: Exploiting the slope of the Brillouin gain spectrum, we develop a new configuration of Brillouin optical correlation-domain reflectometry, which can measure strain (or temperature) and optical loss distributions simultaneously with a high sampling rate. The strain, temperature, and loss dependence coefficients of the output signal are measured to be 1.95×10^{-4} dB/$\mu\varepsilon$, 4.42×10^{-3} dB/K, and 0.191, respectively, which are consistent with the theoretical predictions. We also verify the basic operation of simultaneous measurement of the three parameters.

Index Terms: Brillouin scattering, optical fiber sensors, distributed measurement, correlation-domain techniques.

1. Introduction

To monitor the conditions of civil infrastructures, a variety of fiber-optic distributed strain and temperature sensing techniques based on Brillouin scattering [1] have been extensively studied. They are categorized into two types: "analysis" systems [2]–[19], in which two light beams need to be injected into both ends of a fiber under test (FUT); and "reflectometry" systems [20]–[29], in which only one light beam is injected into one end of the FUT. The former include Brillouin optical time-, frequency-, and correlation-domain analysis (BOTDA [2]–[10], BOFDA [11]–[13], and BOCDA [14]–[19]) systems, while the latter include Brillouin optical time- and correlation-domain reflectometry (BOTDR [20]–[22] and BOCDR [23]–[29]) systems. In analysis systems, stimulated Brillouin scattering with a relatively high reflectivity can be exploited, leading to a high signal-to-noise ratio (SNR) of the measurement. Consequently, extremely high sensing performances, such as an ultimately fast measurement speed in BOTDA [8] and a nominal spatial resolution of as high as 1.6 mm in BOCDA [17], have been reported. However, such two-end-access systems reduce the degree of freedom in embedding the FUT into structures, and they do not function properly when a single breakage occurs in the FUT. From the viewpoint of the users'
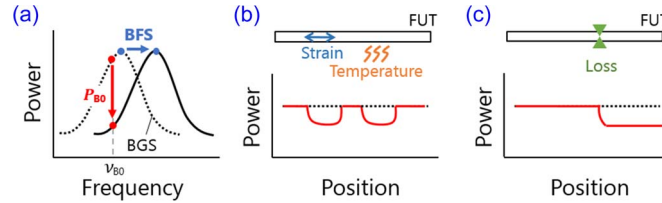
Fig. 1. Schematics of the operating principle of the slope-assisted Brillouin optical correlation-domain reflectometry (SA-BOCDR). (a) One-to-one correspondence between the BFS and the spectral power P_{B0} at frequency ν_{B0}. The dotted curve is the initial BGS, and the solid curve is the BGS shifted to a higher frequency on account of strain and/or heat. (b) P_{B0} distributions along the sensing fiber (solid curve) with and (dotted line) without partial strain and heat. (c) P_{B0} distributions along the sensing fiber (solid curve) with and (dotted line) without a point loss.

convenience, one-end-access reflectometry systems are preferable. Compared to BOTDR, where optical pulses are utilized to resolve the positions, continuous-wave-based BOCDR can achieve a relatively high SNR in principle, leading to a high spatial resolution and a sampling rate.

BOCDR operates based on the correlation control of propagating lightwaves. Even when optical loss occurs in the FUT, conventional BOCDR can provide the Brillouin frequency shift (BFS) distribution properly, which is derived from the Brillouin gain spectrum (BGS) distribution. This feature is an advantage from the aspect of stable strain and temperature measurement; however, in some practical applications, optical loss distribution should be simultaneously obtained.

In this work, to achieve simultaneous distributed measurement of strain (or temperature) and loss, we develop a new BOCDR configuration—named slope-assisted BOCDR (SA-BOCDR) in analogy with SA-BOTDA [5]–[7]—which operates with the assistance of the BGS slope. In this method, the whole BGS need not be observed to derive the BFS value, which potentially leads to a higher sampling (or repetition) rate in principle.

2. Principle

As detailed in [1], BFS in an optical fiber shows strain and temperature dependences, which are often exploited to implement fiber-optic sensors. One of such distributed strain/temperature sensing techniques is BOCDR, which has intrinsic one-end accessibility, a high spatial resolution, a high sampling rate, and cost efficiency. To spatially resolve the sensing locations, we apply sinusoidal frequency modulation to the laser output to generate a so-called "correlation peak" in the FUT [14]. Using the correlation peak, the BFS at a specific position can be selectively detected. By sweeping the modulation frequency f_m, the correlation peak is scanned along the FUT, enabling a distributed BFS measurement. As sinusoidal frequency modulation periodically generates multiple correlation peaks along the FUT, their interval determines the measurement range d_m as [25]

$$d_m = \frac{c}{2nf_m} \tag{1}$$

where c is the velocity of light in vacuum, and n is the refractive index of the fiber core. When f_m is lower than the Brillouin bandwidth $\Delta\nu_B$, the spatial resolution Δz is reported to be given by [25]

$$\Delta z = \frac{c\Delta\nu_B}{2\pi nf_m\Delta f} \tag{2}$$

where Δf is the modulation amplitude of the optical frequency.

In conventional BOCDR systems, the BFS (i.e., strain or temperature) at one sensing point is derived after obtaining the whole BGS. In contrast, SA-BOCDR provides the strain/temperature information using the BGS slope. This scheme has been implemented for BOTDA
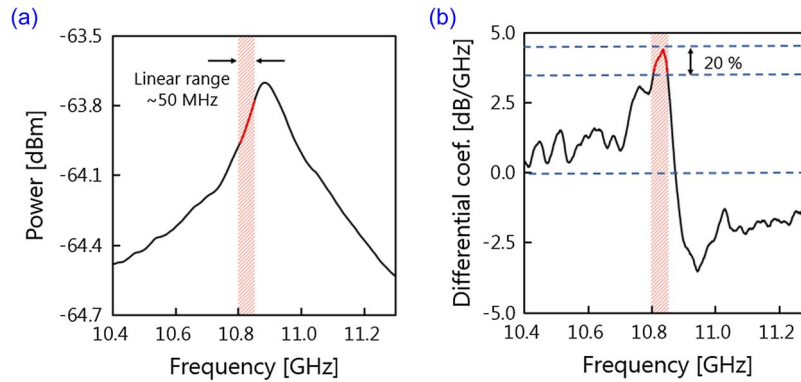
Fig. 2. (a) Measured BGS and (b) its differential coefficient at each frequency. The linear region of the lower frequency side is indicated.

systems [5]–[7]. As depicted in Fig. 1(a), the BFS is in one-to-one correspondence with the spectral power P_{B0} at a certain frequency ν_{B0}, which is set at the high-frequency point in the linear region (lower frequency side) of the BGS slope (see the following paragraph for a quantitative discussion). Then, when the BFS slightly shifts to higher frequency responding to strain and/or heat, P_{B0} decreases linearly; when the slight loss occurs in the FUT, the spectral power of the BGS entirely decreases, also leading to the reduction of P_{B0}. Even if the BFS change is so large that ν_{B0} gets out of the linear region, as long as P_{B0} is in one-to-one correspondence with the BFS, this system operates properly (with a reduced sensitivity) by simple nonlinear compensation. Fig. 1(b) and (c) schematically shows the changes in the P_{B0} distributions when strain (or temperature change) and loss are locally applied, respectively. The strain and temperature effects cannot be separated in this method, but the loss effect can be discriminated from the locally applied strain (or temperature change) because the once decreased P_{B0} value does not return to the initial value (If strain (or temperature change) is applied from a certain point to the distal end of the FUT, it cannot be separated from the point loss; in which case, the problem could be resolved by utilizing the ratio of the spectral powers at two frequencies. The details will be published elsewhere). The P_{B0} change distributions [calculated by substituting the resultant P_{B0} distributions (solid curves) from their initial distributions (dotted lines)] are used as final measurement data.

To evaluate the optimal ν_{B0} value and the bandwidth of the linear region, we analyzed a raw BGS with a BFS of 10.89 GHz [see Fig. 2(a)], which was experimentally obtained when the FUT length L and experimental conditions (such as the modulation frequency f_m and amplitude Δf) were set to the same values as those for the experiment ($L = 5.0$ m, $f_m = 8.0$ MHz, $\Delta f = 1.4$ GHz; refer to the following sections). Here, we define the linear region as the region where the change in the BGS slope is suppressed within 20% compared to its maximum. Based on the slope (i.e. differential coefficient) dependence on the frequency [see Fig. 2(b)] obtained by differentiating the BGS with respect to frequency, the optimal ν_{B0} value to widen the linear region was found to be 10.85 GHz. The bandwidth of the linear region was approximately 50 MHz, which corresponds to the strain of up to $\sim$1035 $\mu\varepsilon$ and the temperature change of $\sim$45 K. In this linear region, the theoretical strain and temperature dependence coefficients were calculated to be 2.11×10^{-4} dB/$\mu\varepsilon$ and 4.27×10^{-3} dB/K, respectively. Note that these coefficients will be different if the experimental conditions alter. For instance, if the spatial resolution is set lower, the coefficients will be larger, while if the video bandwidth (VBW) of an electrical spectrum analyzer (ESA) is set lower, they will be smaller.

3. Experimental Setup

The FUT employed in the experiment was a 5.0-m-long silica single-mode fiber (SMF) with a BFS of 10.89 GHz at 1.55 μm at room temperature. The experimental setup of SA-BOCDR is
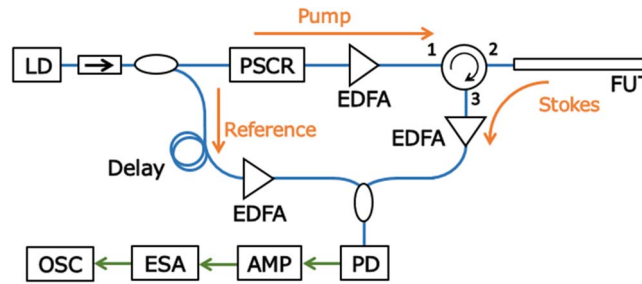
Fig. 3. Experimental setup of SA-BOCDR. AMP, amplifier; EDFA, erbium-doped fiber amplifier; ESA, electrical spectrum analyzer; FUT, fiber under test; LD, laser diode; OSC, oscilloscope; PD, photo diode; PSCR, polarization scrambler.

schematically shown in Fig. 3, which is basically the same as that of conventional BOCDR [23], [25]; the only essential difference lies in the final signal processing. The output light from a distributed-feedback laser diode at 1.55 μm was divided into two light beams, pump and reference. The pump light was amplified to ~24 dBm using an erbium-doped fiber amplifier (EDFA) and injected into the FUT. After passing through a ~1-km-long delay line and another EDFA (amplified to ~5 dBm), the reference light was used for heterodyne detection with the Stokes light, which was amplified to ~2 dBm. The polarization-dependent fluctuations were suppressed using a polarization scrambler. The heterodyned optical signal was converted into an electrical signal using a photo diode and was guided to an ESA (VBW: 3 kHz, resolution bandwidth: 300 kHz). Using the narrowband-pass filtering function of the ESA, the P_{B0} change at a fixed frequency ν_{B0} (= 10.85 GHz) was sequentially output to an oscilloscope (OSC).

A 0.1-m-long section around the distal open end of the FUT was bent to suppress the Fresnel reflection. The modulation frequency f_m and amplitude Δf were set to 7.975–8.055 MHz and 1.4 GHz, respectively, corresponding to the measurement range of 12.9 m and the theoretical spatial resolution of 88 mm from (1) and (2). The repetition rate was 100 Hz, and 16 times averaging was performed on the OSC. The room temperature was 26 °C.

4. Experimental Results

First, we investigated the P_{B0} change dependence on strain. Strains of 0 to 850 $\mu\varepsilon$ were applied to a 0.2-m-long section (3.5–3.7 m away from the circulator) of the FUT. The measured P_{B0} change distributions along the FUT are shown in Fig. 4(a). With increasing strain, the P_{B0} change increased (P_{B0} itself decreased). The P_{B0} change dependence was almost linear in this range [see Fig. 4(b)], and its coefficient was 1.95×10^{-4} dB/$\mu\varepsilon$, which moderately agrees with the theoretical value (2.11×10^{-4} dB/$\mu\varepsilon$). Note that, in Fig. 4(a), the SNR was so low that relatively small strains of $< 300 \mu\varepsilon$ were unable to be distinguished from the signal fluctuations in this measurement.

Subsequently, the P_{B0} change dependence on temperature was measured. The result obtained when the temperature was locally changed to 75 °C in a 0.2-m-long section (2.0–2.2 m) is shown in Fig. 4(c). With increasing temperature, the P_{B0} change increased. The P_{B0} change dependence was almost linear [see Fig. 4(d)] with a coefficient of 4.42×10^{-3} dB/K, which agrees with the theoretical value (4.27×10^{-3} dB/K).

The loss dependence of the P_{B0} change distribution was also measured. Bending losses of 0 to 2.8 dB were applied at a midpoint of the FUT (2.5 m away from the circulator). As shown in Fig. 5(a), with increasing loss, the P_{B0} change increased on the distal side from the loss-applied point (again, note that the P_{B0} value itself decreased). The loss dependence of the P_{B0} change [averaged in the 2.5-m-long distal section (2.5–5.0 m)] was almost linear [see Fig. 5(b)] with a coefficient of 0.191.

We then evaluated the stability of this method. When neither strain/temperature change nor loss was applied to the FUT, we measured the temporal variations of P_{B0} for 20 ms (see Fig. 6). The
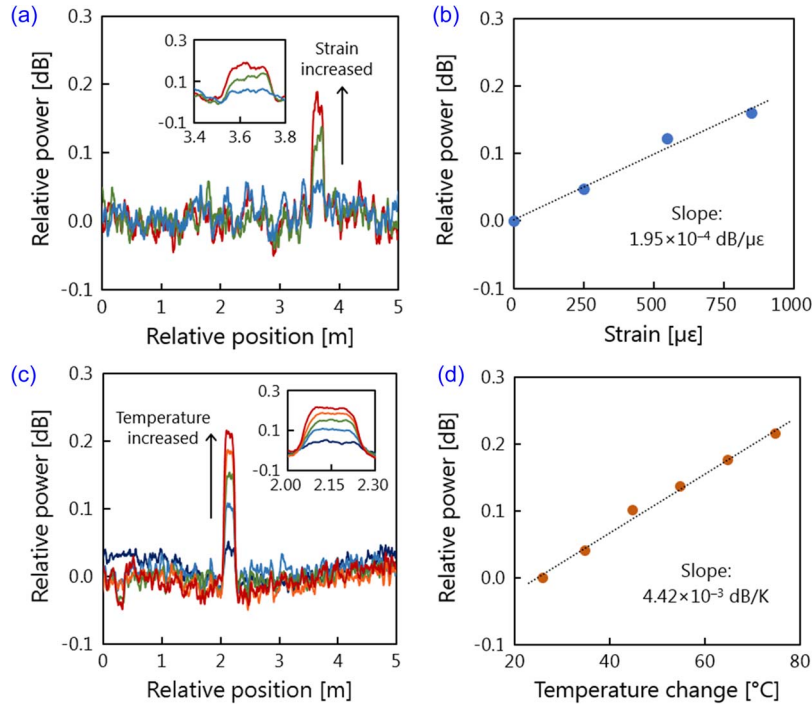
Fig. 4. (a) P_{B0} change distribution when strains were locally applied. (b) P_{B0} change dependence on strain. The dotted line is a linear fit. (c) P_{B0} change distribution when temperature was locally changed. (d) P_{B0} change dependence on temperature. The dotted line indicates a linear fit.
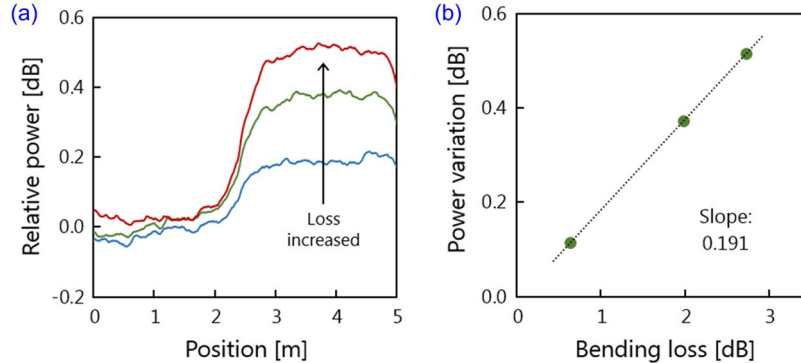

Fig. 5. (a) P_{B0} change distribution when losses were locally applied. (b) P_{B0} change dependence on loss. The dotted line is a linear fit.

standard deviation was calculated to be ~0.0178 dB, which corresponds to a strain error of $+/-92 \ \mu\varepsilon$, a temperature error of +/– 4 K, and a loss error of +/– 0.1 dB. These values, which can be suppressed further by averaging more data at the cost of a reduced sampling (or repetition) rate, showed no quantifiable changes when the measurement time was longer than 10 minutes.

Finally, a proof-of-concept demonstration of SA-BOCDR was performed by simultaneous measurement of strain, temperature, and loss. The structure of the 5.0-m-long FUT is shown in Fig. 7(a); ambient temperature was changed to 55°C along the 1.9–2.1-m section, a 0.64 dB loss was applied at the midpoint, and a 550 $\mu\varepsilon$ strain was applied to the 3.5–3.7-m section. Fig. 7(b) shows the measured P_{B0} change distribution along the FUT. The P_{B0} changes corresponding to the temperature change, loss, and strain were observed at the expected sections. The amounts of
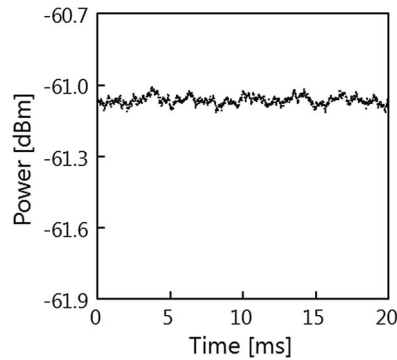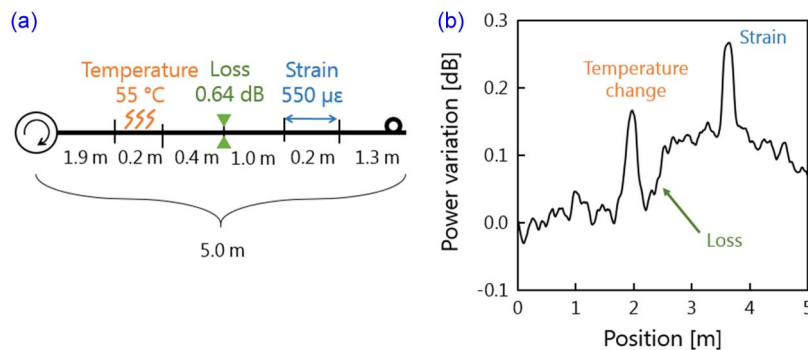
Fig. 6. Measured temporal variations of P_{B0}.

Fig. 7. (a) Structure of the FUT. (b) Measured P_{B0} change distribution.

the P_{B0} changes for the temperature change, loss, and strain were approximately 0.16, 0.14, and 0.12 (= 0.26–0.14) dB (corresponding to the temperature change, loss, and strain of ~62 °C, ~0.73 dB, and $\sim$ 615 $\mu\varepsilon$, respectively). The measurement errors probably originate from the signal fluctuations and the resultant low SNR, which needs to be improved by optimal low-pass filtering and/or increase in the number of averaging in future.

5. Conclusion

We experimentally proved the concept of a new BOCDR configuration, named SA-BOCDR, which can perform the simultaneous distributed measurement of strain (or temperature) and optical loss by exploiting the slope of the BGS. After measuring the strain-, temperature-, and loss-dependence coefficients of the output signal (1.95×10^{-4} dB/$\mu\varepsilon$, 4.42×10^{-3} dB/K, and 0.191, respectively), we verified the basic operation of simultaneous measurement of the three parameters. The improvement of the low SNR is one of the most important future tasks. The limitation of the system performance, such as strain/temperature/loss dynamic ranges, measurement accuracy, and repetition rate, also needs to be clarified.

References

[1] G. P. Agrawal, *Nonlinear Fiber Optics*.   San Diego, CA, USA: Academic, 1995.
[2] T. Horiguchi and M. Tateda, "BOTDA-nondestructive measurement of single-mode optical fiber attenuation characteristics using Brillouin interaction: Theory," *J. Lightw. Technol.*, vol. 7, no. 8, pp. 1170–1176, Aug. 1989.
[3] Z. Li *et al.*, "Coherent BOTDA sensor with single-sideband modulated probe light," *IEEE Photon. J.*, vol. 8, no. 1, Feb. 2016, Art. no. 6800908.
[4] J. Urricelqui, A. Zornoza, M. Sagues, and A. Loayssa, "Dynamic BOTDA measurements based on Brillouin phase-shift and RF demodulation," *Opt. Exp.*, vol. 20, no. 24, pp. 26942–26949, Nov. 2012.

[5] Y. Peled, A. Motil, L. Yaron, and M. Tur, "Slope-assisted fast distributed sensing in optical fibers with arbitrary Brillouin profile," *Opt. Exp.*, vol. 19, no. 21, pp. 19845–19854, Oct. 2011.

[6] X. Tu, H. Luo, Q. Sun, X. Hu, and Z. Meng, "Performance analysis of slope-assisted dynamic BOTDA based on Brillouin gain or phase-shift in optical fibers," *J. Opt.*, vol. 17, no. 10, Sep. 2015, Art. no. 105503.

[7] A. Minardo, A. Coscetta, R. Bernini, and L. Zeni, "Heterodyne slope-assisted Brillouin optical time-domain analysis for dynamic strain measurements," *J. Opt.*, vol. 18, no. 2, Jan. 2016, Art. no. 025606.

[8] I. Sovran, A. Motil, and M. Tur, "Frequency-scanning BOTDA with ultimately fast acquisition speed," *IEEE Photon. Technol. Lett.*, vol. 27, no. 13, pp. 1426–1429, Jul. 2015.

[9] L. Thevenaz, S. F. Mafang, and J. Lin, "Effect of pulse depletion in a Brillouin optical time-domain analysis system," *Opt. Exp.*, vol. 21, no. 12, pp. 14017–14035, Jun. 2013.

[10] Y. Dong *et al.*, "High-spatial-resolution fast BOTDA for dynamic strain measurement based on differential double-pulse and second-order sideband of modulation," *IEEE Photon. J.*, vol. 5, no. 3, Jun. 2013, Art. no. 2600407.

[11] D. Garus, K. Krebber, and F. Schliep, "Distributed sensing technique based on Brillouin optical-fiber frequency-domain analysis," *Opt. Lett.*, vol. 21, no. 17, pp. 1402–1404, Sep. 1996.

[12] R. Bernini, A. Minardo, and L. Zeni, "Distributed sensing at centimeter-scale spatial resolution by BOFDA: Measurements and signal processing," *IEEE Photon. J.*, vol. 4, no. 1, pp. 48–56, Feb. 2012.

[13] A. Wosniok, Y. Mizuno, K. Krebber, and K. Nakamura, "L-BOFDA: A new sensor technique for distributed Brillouin sensing," in *Proc. 5th EWOFS*, Krakow, Poland, 2013, pp. 8794–8798.

[14] K. Hotate and T. Hasegawa, "Measurement of Brillouin gain spectrum distribution along an optical fiber using a correlation-based technique—Proposal, experiment and simulation," *IEICE Trans. Electron.*, vol. E83-C, no. 3, pp. 405–412, Mar. 2000.

[15] R. Cohen, Y. London, Y. Antman, and A. Zadok, "Brillouin optical correlation domain analysis with 4 millimeter resolution based on amplified spontaneous emission," *Opt. Exp.*, vol. 22, no. 10, pp. 12070–12078, May 2014.

[16] C. Zhang, M. Kishi, and K. Hotate, "5,000 points/s high-speed random accessibility for dynamic strain measurement at arbitrary multiple points along a fiber by Brillouin optical correlation domain analysis," *Appl. Phys. Exp.*, vol. 8, no. 4, Mar. 2015, Art. no. 042501.

[17] K. Y. Song, Z. He, and K. Hotate, "Distributed strain measurement with millimeter-order spatial resolution based on Brillouin optical correlation domain analysis," *Opt. Lett.*, vol. 31, no. 17, pp. 2526–2528, Aug. 2006.

[18] J. H. Jeong *et al.*, "Linearly configured BOCDA system using a differential measurement scheme," *Opt. Exp.*, vol. 22, no. 2, pp. 1467–1473, Jan. 2014.

[19] D. Elooz, Y. Antman, N. Levanon, and A. Zadok, "High-resolution long-reach distributed Brillouin sensing based on combined time-domain and correlation-domain analysis," *Opt. Exp.*, vol. 22, no. 6, pp. 6453–6463, Mar. 2014.

[20] T. Kurashima, T. Horiguchi, H. Izumita, S. Furukawa, and Y. Koyamada, "Brillouin optical-fiber time domain reflectometry," *IEICE Trans. Commun.*, vol. E76-B, no. 4, pp. 382–390, Apr. 1993.

[21] A. Masoudi, M. Belal, and T. P. Newson, "Distributed dynamic large strain optical fiber sensor based on the detection of spontaneous Brillouin scattering," *Opt. Lett.*, vol. 38, no. 17, pp. 3312–3315, Sep. 2013.

[22] D. Iida and F. Ito, "Detection sensitivity of Brillouin scattering near Fresnel reflection in BOTDR measurement," *J. Lightw. Technol.*, vol. 26, no. 4, pp. 417–424, Feb. 2008.

[23] Y. Mizuno, W. Zou, Z. He, and K. Hotate, "Proposal of Brillouin optical correlation-domain reflectometry (BOCDR)," *Opt. Exp.*, vol. 16, no. 16, pp. 12148–12153, Jul. 2008.

[24] N. Hayashi, Y. Mizuno, and K. Nakamura, "Distributed Brillouin sensing with centimeter-order spatial resolution in polymer optical fibers," *J. Lightw. Technol.*, vol. 32, no. 21, pp. 3397–3401, Nov. 2014.

[25] Y. Mizuno, W. Zou, Z. He, and K. Hotate, "Operation of Brillouin optical correlation-domain reflectometry: Theoretical analysis and experimental validation," *J. Lightw. Technol.*, vol. 28, no. 22, pp. 3300–3306, Nov. 2010.

[26] N. Hayashi, Y. Mizuno, and K. Nakamura, "Brillouin gain spectrum dependence on large strain in perfluorinated graded-index polymer optical fiber," *Opt. Exp.*, vol. 20, no. 19, pp. 21101–21106, Sep. 2012.

[27] Y. Mizuno, Z. He, and K. Hotate, "Measurement range enlargement in Brillouin optical correlation-domain reflectometry based on double- modulation scheme," *Opt. Exp.*, vol. 18, no. 6, pp. 5926–5933, Mar. 2010.

[28] N. Hayashi, Y. Mizuno, and K. Nakamura, "Simplified Brillouin optical correlation-domain reflectometry using polymer optical fiber," *IEEE Photon. J.*, vol. 7, no. 1, Feb. 2015, Art. no. 6800407.

[29] Y. Mizuno, Z. He, and K. Hotate, "One-end-access high-speed distributed strain measurement with 13-mm spatial resolution based on Brillouin optical correlation-domain reflectometry," *IEEE Photon. Technol. Lett.*, vol. 21, no. 7, pp. 474–476, Apr. 2009.